Received 26 July 2022; revised 14 August 2022; accepted 22 August 2022. Date of publication 29 August 2022; date of current version 8 September 2022.

Digital Object Identifier 10.1109/OJAP.2022.3201627

A 5G Enabled Shared-Aperture, Dual-Band, In-Rim Antenna System for Wireless Handsets

REZA SHAMSAEE MALFAJANI (Graduate Student Member, IEEE), FARHAD BIN ASHRAF, AND MOHAMMAD S. SHARAWI, (Senior Member, IEEE)

Department of Electrical Engineering, Polytechnique Montreal, Montreal, QC H3T 1J4, Canada

CORRESPONDING AUTHOR: M. S. SHARAWI (e-mail: mohammad.sharawi@polymtl.ca)

This work was supported in part by the Fonds de recherche du Québec Nature et technologies (FRQNT) under Grant 2022-PR-298793, and in part by the Natural Sciences and Engineering Research Council of Canada under Project RGPIN-2019-05298.

ABSTRACT In this work, we present a shared aperture (SA), dual-band in metal-rim antenna system targeting the sub-6GHz and millimeter-wave (mm-wave) bands of the 5G wireless standard. The antenna system consists of a SA cactus-shaped slot engraved on the side of standard mobile terminal rim that hosts a microwave radiating structure covering the sub-6 GHz bands as well as a 4-element slot based connected antenna array (SB-CAA) covering the mm-wave bands. This provides a compact sized solution for multiband operation within these bands. The CAA has beam forming capabilities where the beam can be steered between +/− 30 degrees with acceptable gain and side lobe levels (SLL). A single 4-element slot based in-rim SB-CAA is also proposed that covered more than 6 GHz of frequency bandwidth (25.5–32 GHz) with a total efficiency exceeding 85% and realized averaged gain of 8.2 dBi over the bands covered. The SA cactus antenna structure had a bandwidth exceeding 3.5 GHz with total efficiency exceeding 75% and an average realized gain of 8 dBi between 26.5 – 30 GHz. For the microwave band covered (3.45-3.56 GHz) by this SA cactus antenna, a bandwidth of 140 MHz, efficiency of 90% with 2.5 dBi of measured gain were achieved.

INDEX TERMS Shared aperture antenna (SAA), beam steering, connected antenna array (CAA), in-rim antenna, millimeter-wave (mmWave), slot.

I. INTRODUCTION

DUE TO the rapid development in wireless communication technologies and applications, there is growing demand for high-end mobile devices with many flagship features. Advanced mobile communication technology is urgently demanded to offer a higher throughput, shorter latency, and lower energy consumption for fifth generation (5G) mobile communications. 5G offers a new network architecture to help significantly boost overall performance compared to its fourth generation (4G) predecessor. The introduction of the millimeter-waves (mm-wave) bands has been a key for achieving the high data rates promised by 5G. The introduction of mm-wave antenna modules and arrays will make the volume and space requirements even more challenging when designing a handheld terminal due to the large frequency gap between sub-6 GHz and mm-wave bands [1].

Metal-rimmed smartphone designs have attracted much attention in recent years, because of their enhanced mechanical strength and aesthetic appearance without any additional volume for antennas (efficient space utilization). Connected antenna arrays (CAAs) are potential candidates for 5G smartphone antenna designs. CAAs can provide wider bandwidths, lower cross-polarization levels, better gains, and smaller sizes on metal rims when designed properly. They provide wideband characteristics as the connections between adjacent elements yield constant currents [2]. CAA will also occupy less space as compared to other antenna types, thus allowing for more integration and higher array densities.

The introduction of 5G devices operating at mm-wave frequencies has raised significant challenges for the communication industry, particularly for handheld devices. The use of metal-rimmed antennas as slots has been implemented in mobile antennas to achieve multiband operation [3], [4], [5].

Dual-polarized, end-fire chain slot antenna array were reported in [4], [5], [7]. In [3], a large metal ground and an unbroken metal rim was used to achieve multiband operations as 4G (820–960 and 1710–2690 MHz) and 5G (3400–3600 MHz). In [5], a dipole antenna operated at mm-wave band (23 to 29 GHz) through a 20×3.5 mm^2 window was proposed. It had a beam-steering capability up to $\pm40°$ using a three-element array. Choi *et al.* in [6] proposed a 1×4 planar folded slot antenna (PFSA) subarray with a multi throw topology demonstrated frequency adjustment from 27.95 to 28.65 GHz. It featured a 2.6-time enhanced impedance bandwidth and an average peak gain of 6.3 dBi.

The colocation of the microwave and mm-wave antennas is a major challenge due to the limited space available in the handset. To address the challenges of multi-band operation and colocation with lower bands (4G or 5G based), several promising designs were proposed to cover both microwave and mm-wave bands [8], [9], [10], [11], [12], [13], [14], [15]. However, all the above-mentioned designs have their own restrictions. In [9] and [10] the authors were unable to cover mm-wave bands (due to large band difference between sub-6 GHz and mm-wave at 28 GHz). In [11] and [13], two designs were presented with good performance at microwave and mm-wave bands. But they were built on multi-substrates which is complicated and less cost effective. Moreover, both were reported with relatively low gain at the mm-wave band, and both used different radiating structures for the two bands. Dual-functional connected slots were presented in [10] and [12] for 4G and 5G applications. Connected slots were used both as an isolation enhancement structure between microwave antennas and as antenna array at mm-wave band. Those designs used two different structures to cover microwave and mm-wave bands therefore they occupied relatively large amount of the board eventually making them less suitable for handsets. In [8], a dual-function slot antenna operated at both microwave and mm-wave bands was proposed. The designed slot had dual functionality, it worked as a tunable slot antenna at 4G microwave band and operates as a wideband antenna array at 5G mm-wave band using the principle of CAA. The tunable slot antenna had a bandwidth from 2.05 to 2.70 GHz with 45-70% efficiency and 4.5 dBi of peak realized gain. The wideband CAA had a bandwidth from 23 to 29 GHz with 12.5 dBi realized gain and 80-90% measured efficiency.

An aperture-sharing methodology was proposed in [14], they presented a four linear array antenna at 28 GHz array along with a 3.5 GHz dipole antenna that are using the same aperture to resonant. A double-sided parallel strip line (DSPSL) was used to feed the double-sided dipole antenna, by using this method they incorporated the mm-wave antenna array. At mm-wave band, a double-sided interdigital coupling (IDC) structure was introduced into each DSPSL to achieve broad bandwidth by implementing indirect coupling. The overall structure size was $33.9\times43\times0.254$ mm^3 and the reported gain of the mm-wave array and 3.5 dipole antenna varies from 5.8 to 7.5 dBi and 6.1 to 6.9 dBi over the BW, respectively. They reported approximately 20% impedance bandwidth in both bands. The beam steering capabilities of the structure was limited to 0° and 25° in the E-plane because they used two different fixed feeding networks for the 28 GHz array antenna. Another aperture sharing broadside antenna was investigated in [15]. A substrate-integrated DRA (SIDRA) with a 2×4 configuration at 26 GHz and a segmented patch antenna at 3.5 GHz was utilized in an aperture shared way. They reported three benefits: compact size, size adaptation of SIDRA with the patch antenna and high integrity level. Separate feeding network was applied to accomplish independent excitation and radiation pattern. They reported a 12.3% BW at microwave band and a 13.1% at mm-wave band with 5.3 and 15.4 dBi peak gain respectively. Their measured beam steering capabilities are also limited to 0° and 25°. Multilayered structure and use of DRA make it complex antenna for 5G mobile phone.

A relatively new concept has been developed because of the space availability for the antennas in handheld devices. In the antenna in antenna (AiA) concept, two antennas are incorporated in such a way that one antenna structure operates in a frequency band that is used and shared with the second antenna operating in a different frequency band. A dual-band mm-wave antenna array working at 28 GHz and 39 GHz for the 5G was proposed in [16]. They used two interconnected slots of different length to enable the integrated design with a metal rim of a handset and claimed it as a promising solution of AiA concept. The simulation results showed bandwidth from 27.4 to 29.6 GHz and from 36.9 to 40.2 GHz to cover the 5G mm-wave bands of n260 and n261. The maximum scan angles were $\pm60°$. In [17], an AiA was proposed for sub-6 and mm-wave bands based on a 5-element stacked patch array that is also tuned via external components to serve as 2.4 GHz LTE antenna.

In this work, the design of a compact, in-rim cactus shaped SB-CAA antenna system covering both sub-6 GHz and mm-wave bands for 5G enabled terminals is proposed. The antenna system is an integration between a microwave structure and a mm-wave SB-CAA utilizing shared aperture antenna (SAA) concepts. The proposed SAA covers the 3.45–3.56 GHz and 26.5–30 GHz bands. The 4-element CAA within this SAA provides $+/-30$ degrees of beam steering capability. In addition, a single SB-CAA structure is designed covering mm-wave bands 25.5–32 GHz with very high efficiencies (more than 80%). The proposed solution is unique in its geometry, complexity, covered bands, size, and beam-steering capabilities compared to others, making it a potential candidate in future wireless handheld devices.

The rest of the paper is organized as follows; Section II presents the design details of the single SB-CAA and the design steps of the cactus shaped SAA. In Section III, the measurement results of the fabrication prototypes are presented and compared with their simulation counterparts.

A table of comparison with state of the art is presented as well. Section IV concludes the paper.

II. DESIGN AND ANALYSIS OF THE ANTENNA SYSTEMS

A. SINGLE SLOT-BASED CONNECTED ANTENNA ARRAY (SB-CAA)

An array of 2 or more antennas which are electrically connected is called a CAA. It provides wideband characteristics as the connections between adjacent elements yields nearly constant currents where narrow-band unconnected dipoles have sinusoidal and frequency dependent ones. CAA will also occupy less space as compared to other antenna types, thus allowing for more integration and higher array densities. Another attractive feature of CAA is their capability to achieve good polarization purity, in virtue of the planarity of the radiating currents. Detailed relationships governing the impedance behavior of such structures can be found in [18].

The proposed single slot CAA system was modeled and simulated using CST Microwave Studio 2019. A single slot (17.8 mm x 2 mm) is cut in the middle of a metal frame structure (lossy copper with σ = 5.8 x 107 S/m). A half wavelength single slot resonating at 28 GHz will have a width of approximately 5.3 mm, and when connected together to form a CAA, the combined continuous slot yields a 4-element linear array with smaller size than the original individual ones. To reduce the simulation time, only a portion of the metal rim frame is considered. The metal rim is 50 mm in length, 8.4 mm in width and 1 mm in thickness (representing a commercial smart phone rim width and thickness). To feed the slot antenna, a microstrip feedline offset at $\lambda/20$ is used to have proper impedance matching. The slot antenna is designed to represent a SB-CAA with 4 elements fed by four microstrip feedlines. The antenna array is designed with a center frequency of 28 GHz and is intended to be places on any of the metal rim sides.

Fig. 1 shows the structure of this 4-element SB-CAA and its feeding mechanism. A stage (exploded) view is also shown in Fig. 1(c) to have a full understanding of the structure. An RO3003 substrate is used that had a relative permittivity of $\varepsilon r = 3$, loss tangent of tanδ=0.001 and thickness of 0.25 mm. The inter-element spacing between the feedlines is kept $\lambda 0/2$. The microstrip feedline is 3.9 mm in length from the bottom edge of the rim. A backing reflector (BR) is placed behind the single SB-CAA. A box is created to mimic the actual environment inside the smartphone where display, battery and other ICs are normally placed. The BR is placed $\lambda 0/4$ away from the slot antenna to improve the pattern directivity out of the slot. Its width has been optimized to 38 mm and its sides were extended to be tightly attached to the rim via the side screws as a good GND connection is vital to the proper operation of the antenna (loose connections will affect the matching as well as the purity of the patterns). The thickness of the BR metal is 0.2 mm. The overall PCB dimensions were 17.13×50×0.25 mm3 and the rim slot was filled with air. The substrate is bent by 90o in order to accommodate it

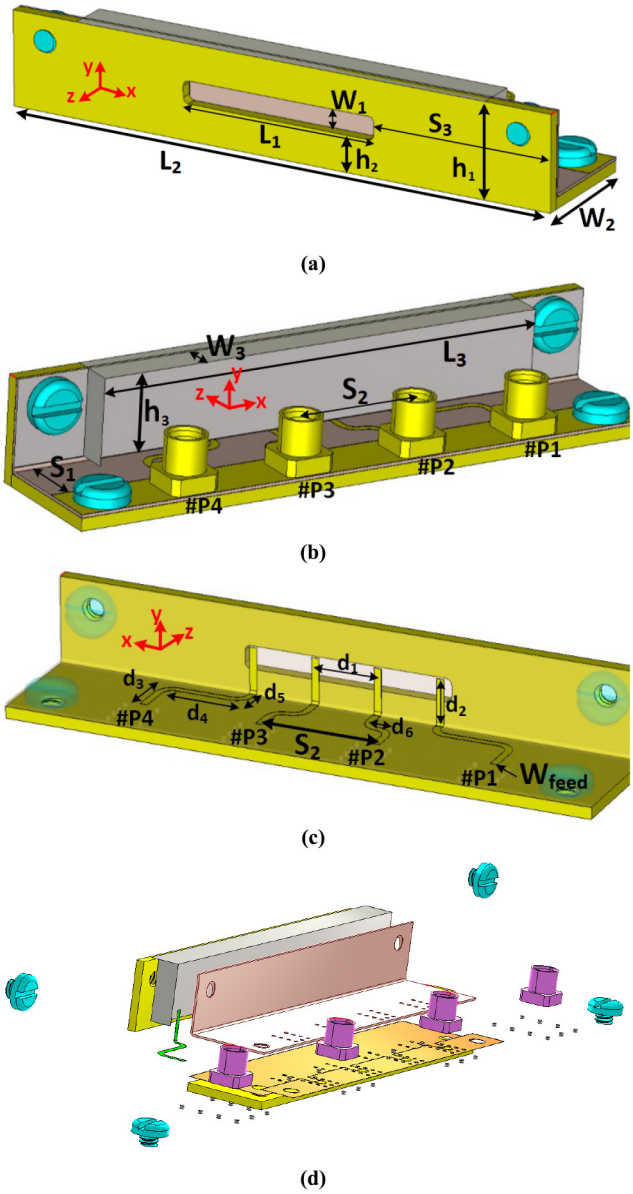

FIGURE 1. Single 4-element SB-CAA design details (a) Geometry of single slot antenna with BR. (b) Back view of the structure with BR showing the feeding lines and mini-smp connectors, (c) Back view of the structure without BR or connectors and showing the feeding lines (d) Stage (exploded) view of a single SB-CAA.

in the mobile phone frame. The feedline is extended at the base, to place the mini-SMP connectors (PE44489). Four nylon screws are placed to hold the board into the metal rim. Vias are also used to make strong ground connections beneath the connectors.

A complete parametric sweep analysis for optimizing the dimensions of the SB-CAA antenna was conducted. The effect of the three main design parameters, i.e., slot length (*L1*), slot width (*W1*) and distance between periodic feedlines (*d1*) are shown for ports 1 and 2 in Fig. 2. Note that the structure is symmetric and thus the behavior of ports 3 and 4 will closely follow those of ports 1 and 2. The swept values show the effect of the parameters on the resonance,

TABLE 1. Values of different geometrical parameters for SB-CAA antenna.

Parameter	Value (mm)	Parameter	Value (mm)
d1	5.3	**L1**	17.8
d2	3.9	**L2**	50
d3	4.1	**L3**	38
d4	7	**S1**	5.1
d5	1.4	**S2**	10
d6	2.3	**S3**	16.1
h1	8.4	**W1**	2
h2	3.2	**W2**	11
h3	6.1	**W3**	2.4
Wfeed	0.63		

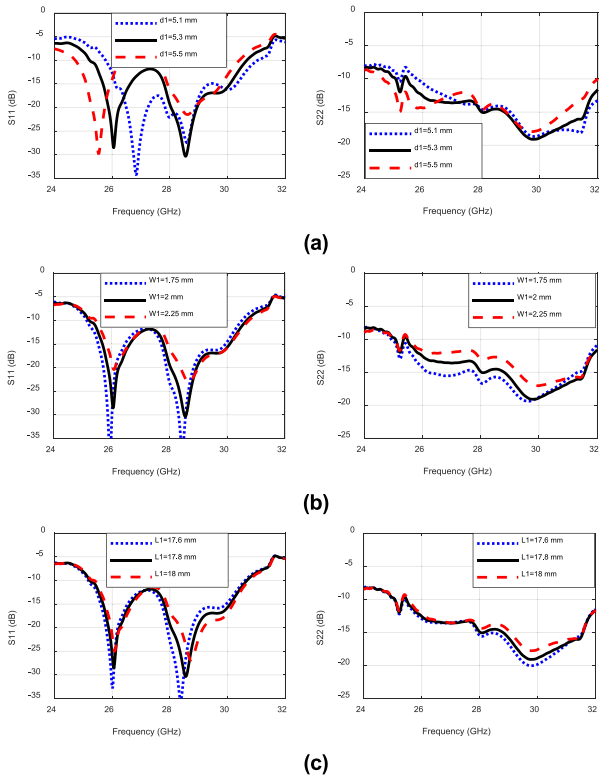

FIGURE 2. Single slot CAA analysis, (a) effect of the feed line spacing (d1), (b) effect of the slot width (W1), (c) effect of slot length (L1).

bandwidth, and matching levels. A compromise with best values for each while fixing others was conducted. Best compromise curves are identified with black color. The final results of the parametric sweeps are summarized in Table 1. The table shows the optimized values from such sweeps and these values for the various dimensions and parameters were used in all upcoming simulations and the fabricated prototype. Initial values for the parameters were assumed with some coarse sweeps, and then finer value sweeps were made to close down on the optimum dimensions.

B. SHARED APERTURE CACTUS-BASED ANTENNA (SA-CACTUS)

5G mobile network has two allocated frequency bands, sub-6 GHz and mm-wave bands. The SA concept is a new

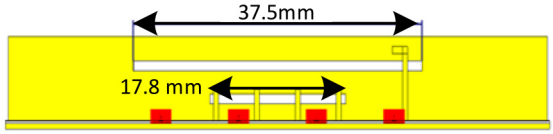

FIGURE 3. Dual-band lot antennas with two separate apertures (slots); one for sub-6GHz (long) and another for mm-wave CAA (short).

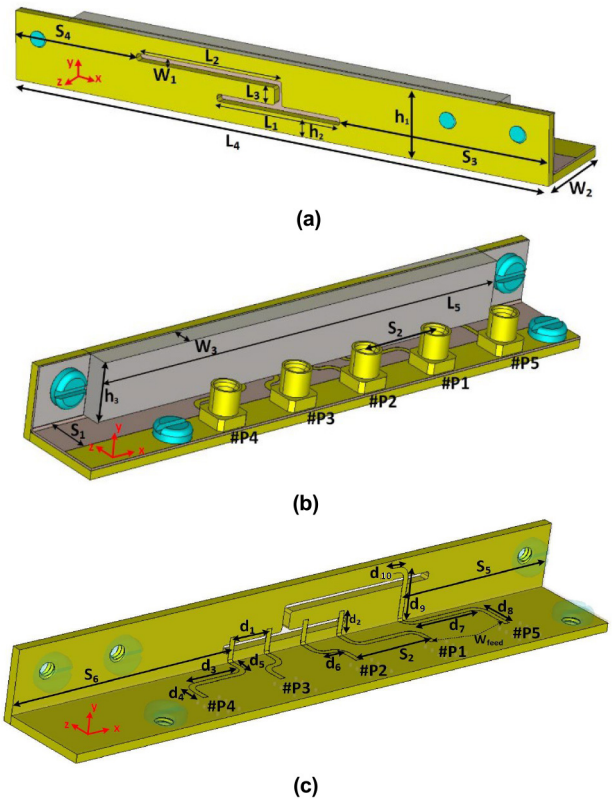

FIGURE 4. Geometry of the SA cactus shaped antenna, (a) front view, (b) Back view of the structure with BR and mini-smp connectors. (c) Back view without BR or connectors.

approach to achieve compact antennas with multi-band operation. To resonant at sub-6 GHz, a very long slot has to cut in the metal rim. To resonant at 3.5 GHz, the slot should be 37.5 mm long (i.e., around half wavelength) which will use a large area of the metal rim as shown in Fig. 3 (also shown is a 4-element CAA slot for mm-wave operation). Practically, it is not viable nor recommended to use such an antenna. Instead of a large slot, the aperture of an existing slot at mm-wave bands (such as the one shown in Section II-A) can be combined to share its aperture with a partial size of the required standard microwave slot operating at sub-6 GHz. The proposed SA structure is shown in Fig. 4. The original standard large slot required to resonant at 3.5 GHz (top slot in Fig. 3) is cut almost by half and is then connected with the mm-wave slot to form a cactus shaped slot (hence the name). The middle location was chosen for best matching and to provide symmetric current around the mm-wave slot. Now the cactus shaped slot will be used to resonate at 3.5 GHz, while the smaller slot will

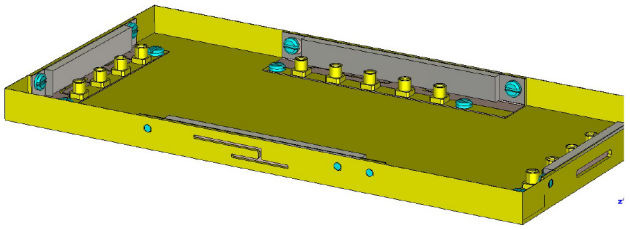

FIGURE 5. Complete metal frame view with the two antenna models, the SB-CAA and the SA cactus based. Two of each design are shown on opposite edges.

TABLE 2. Values of different geometrical parameters of the SA-cactus antenna.

Parameter	Value (mm)	Parameter	Value (mm)
d1	4.8	**L1**	16.1
d2	2.8	**L2**	19.2
d3	7.8	**L3**	2.1
d4	3.2	**L4**	70
d5	2.4	**L5**	56
d6	2.6	**S1**	5.08
d7	9.7	**S2**	10
d8	4.7	**S3**	27
d9	6.4	**S4**	16.3
d10	2.9	**S5**	19.4
h1	8.4	**S6**	27.6
h2	2.3	**W1**	0.9
h3	6.7	**W2**	11
Wfeed	0.63	**W3**	2.4

continue to serve as the mm-wave band SB-CAA. To feed the 3.5 GHz slot antenna a separate microstrip feedline is used with an extended portion for better impedance matching. To accommodate the new slot, feedline and mini-SMP connector, the length of the PCB board increased to 70 mm as compared to the single SB-CAA shown in Section II-A, but the area of the SA-cactus slot antenna reduced significantly on the rim (compare with [20] that occupies a much larger area). RO3003 was used with the same thickness as for the single slot design to feed the cactus shaped one. By this approach, a new SA in-rim antenna system is proposed for 5G mobile handsets that can operate at both microwave and mm-wave bands with beam steering capabilities. The final complete metal frame (rim) with the two antennas the SB-CAA and the SA cactus is shown in Fig. 5.

Again, a comprehensive parametric sweep analysis has been conducted to identify the best combination of dimensions to achieve the widest bandwidth, best impedance matching and proper efficient radiation. Some of the main parameters swept are shown in Fig. 6. For example, the parametric sweeps of the dimensions *L1*, *W1*, *L2*, *L3*, and *d1* are shown. The black curves show the best compromise between the various parameters and sweeps made. Microwave band sweeps are not shown as they are less sensitive to small variations and the extension of L2 will simply shift the resonance downwards. The dimensions of the final structure shown in Fig. 4 are presented in Table 2. The BR needs good connectivity with the metal frame, and thus it was extended from the two sides to attach it with screws to the rim. The BR length is (56 mm).

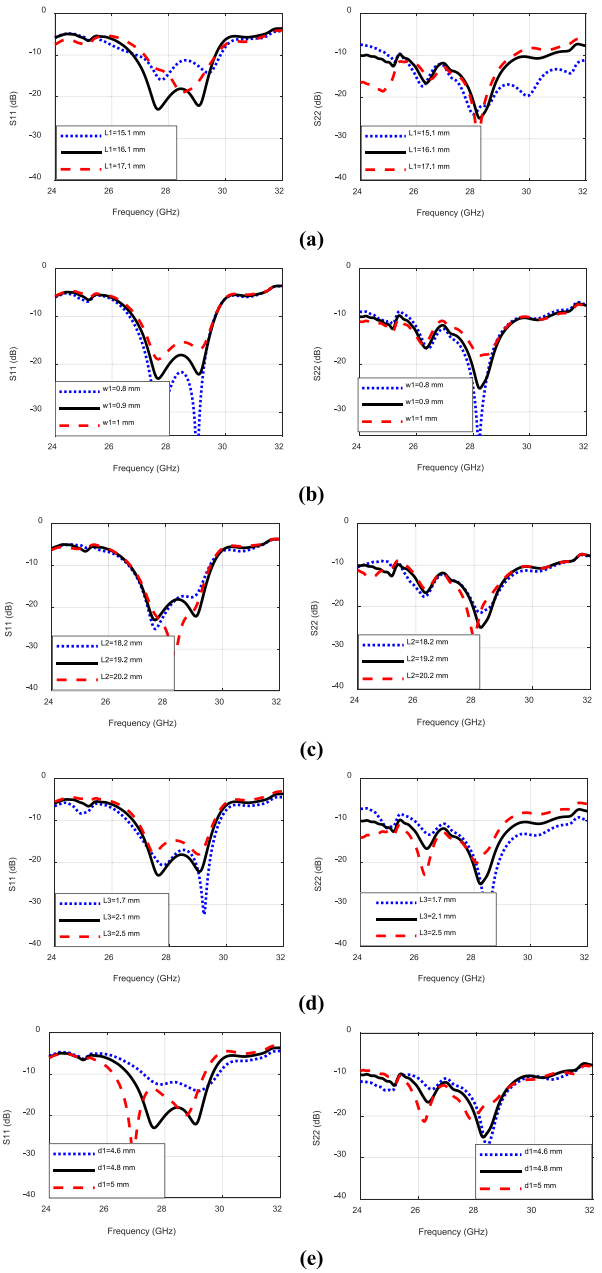

FIGURE 6. Analysis of SA cactus shaped antenna for ports 1 and 2, (a) effect of *L1*, (b) effect of *W1*, (c) effect of *L2*, (d) effect of *L3* (e) effect of *d1*.

C. CURRENT DISTRIBUTIONS OF THE SA CACTUS ANTENNA

The current distribution of the SA Cactus antenna is shown in Fig. 7. As can be seen, when port #5 is excited, the current is circulated around all the aperture of the cactus slot (top and bottom), indicating a lower frequency band resonance around 3.5 GHz. The electrical length of the current path is around 36 mm (close to the separate long slot of 37.5 mm shown in Fig. 3, corresponding to around $\lambda_0/2$ around 4GHz. But recall that the feeding position, matching stub as well as the metal thickness will slightly shift this value from 4GHz

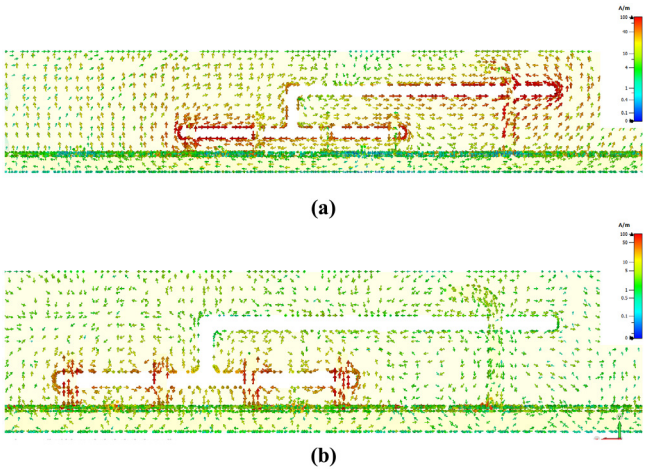

FIGURE 7. Current distribution of the SA Cactus antenna (a) when port 5 (sub-6 GHz) is active and (b) when ports 1, 2, 3 and 4 (mm-wave) are active.

downwards). And when ports 1 to 4 are excited for the mm-wave part (CAA), the current in the upper slot is not strong, rather the current is trapped in the lower slot of the structure representing the operation in the higher band.

III. RESULTS AND DISCUSSIONS

In this section, we will present the simulated and measured results from the prototypes built for each antenna configuration. All modeling and simulation results were obtained using CST software package. The simulated results were extracted with the complete frame structure for proper comparison with the fabricated one (see Figs. 4 and 5). The overall size of the metal frame is 147×72×8.4 mm3 and the metal is 1mm thick. The S-parameters were measured using a Keysight PNA N5224B while the radiation patterns were measured in two chambers, the sub-6 GHz bands were measured in a Satimo Star-Lab system while the mm-wave bands were measured in a quasi-far field chamber at the Poly-Grames research center, Polytechnique Montréal.

A. FABRICATED PROTOTYPES

Fig. 8 shows the various parts of the fabricated prototype for the SA cactus shaped antenna. The single SB-CAA structure had the same fabrication steps and boards. One complete metal frame was custom build and machined using Brass H59 (with $\sigma \sim 2$ x 107 S/m) where the single SB-CAA was created at the top and bottom short sides, and the cactus SA antenna was placed on the left and right longer sides of the mobile metal frame (rim). Note that also we have machined a metal plate (aluminum) with thickness of 2 mm to press down the thin feeding network RO3003 boards, and make sure that the mini-SMP connectors are well situated to avoid being popped out or bending the feeding board (due to its 0.25 mm thickness). Fig. 8(a) shows the feeding network with the single port sub-6 GHz line, and the 4-element mm-wave connectors. Fig. 8(b) shows the bottom side with the SA cactus antenna made to be placed back-to-back with

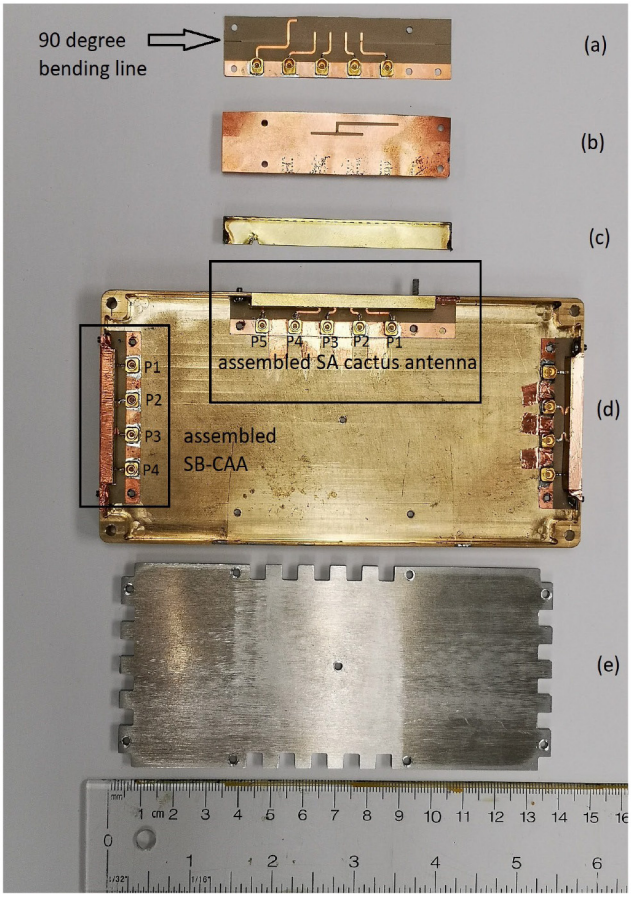

FIGURE 8. Fabricated prototype exploded view (a) feeding network board with connectors and lines on top side, (b) feeding network board bottom side with the SA-cactus for alignment with the metal rim, (c) metallic backing reflector, (d) assembled feeding networks for the two antenna structures, (e) metal plate for better board attachment to the base.

the metal rim for alignment purposes. Fig. 8(c) shows the metallic backing reflector. Fig. 8(d) shows the top view of the mobile terminal metal frame showing two assembled antennas, the single SB-CAA and the SA cactus one. Finally, Fig. 8(e) shows the metal plate used to hold down the boards and connectors as well as serving as a battery/electronics behind the antenna assemblies.

A custom-made plastic holder was also made to hold the cables (086-KM+) as well as stabilize the 2.92 mm to min-SMP adapters (SM8921) and avoid their bends while measuring the S-parameters as well as the radiation patterns. Fig. 9(a) shows this plastic holder in action while performing various measurements. A Side view of the fabricated and assembled antenna system (with both antenna types) can be side of its side in Fig. 9(b).

B. RESULTS FOR THE SINGLE SB-CAA ANTENNA

The measured and simulated S-parameters of the single SB-CAA are shown in Fig. 10. Due to the symmetry of the mm-wave slot, and the fact that elements 1 and 4 have different boundary conditions (as compared to 2 and 3 that see open symmetric boundary conditions on both sides), we can

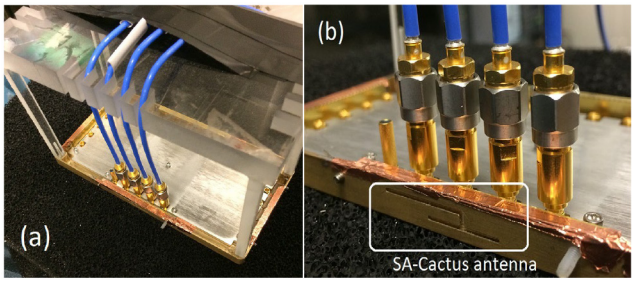

FIGURE 9. Fabricated plastic holder with the metal frame and connected cables, (a) metal frame inside the plastic holder with cables connected, (b) zoomed in view on the SA-Cactus antenna side.

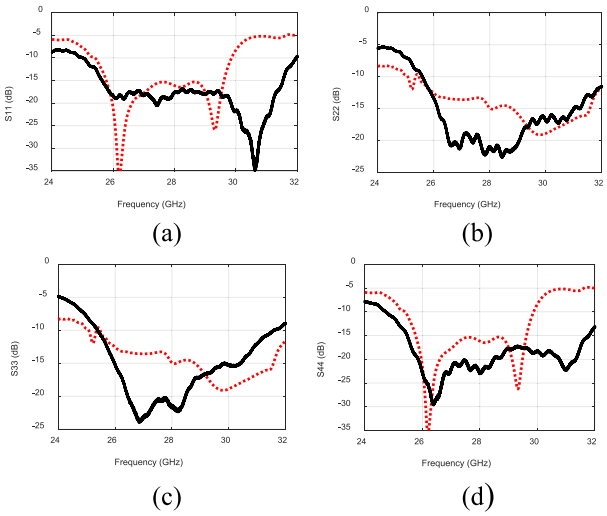

FIGURE 10. S-parameters for the single SB-CAA, dashed are simulated curves, solid are measured curves (a) port 1, (b) port 2, (c) port 3 and (d) port 4.

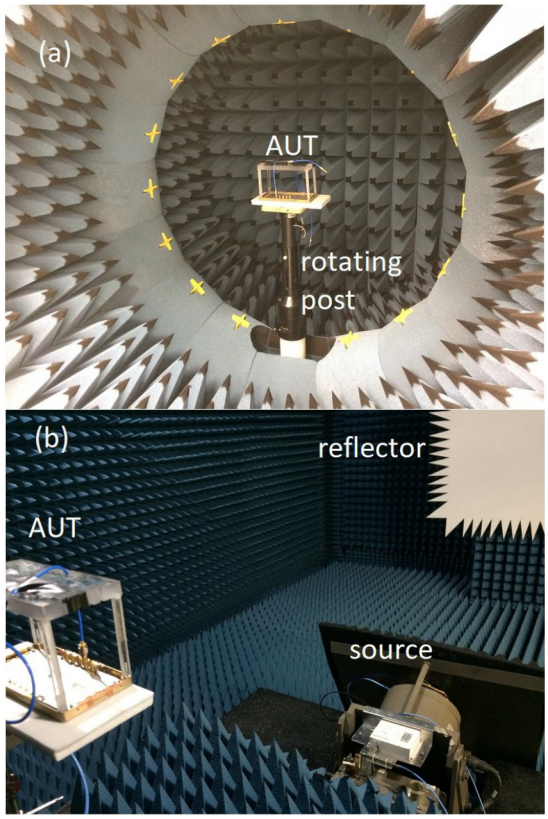

FIGURE 11. Measurement setups, (a) SA cactus antenna at 3.5 GHz, (b) SB-CAA and SA cactus based arrays at mm-wave bands.

see that the behavior of elements 1 and 4 and elements 2 and 3 are similar. Looking at elements (ports) 1 and 4, the simulation results show a frequency bandwidth of approximately 4.4 GHz (25.4 – 29.8 GHz), while the measured bandwidth was wider and provided around 6 GHz of bandwidth. This discrepancy can be related to the slight differences in the fabricated and measured models, which might have resulted in a resonance around 31 GHz close to the edges, in addition to the slight difference in the material and frame properties (i.e., the simulated rim was lossy copper while the fabricated one was Brass H59 with unknown exact electrical properties). The simulated and measured responses for elements 2 and 3 were better matched due to the open-ended boundary conditions that were not close to the fabrication and soldering effects. The simulated bandwidth was around 6.5 GHz (25.5-32 GHz) while the measured bandwidth was around 6.2 GHz (25.4 – 31.6 GHz). For CAA, the isolation between the ports is not considered, as high coupling is expected due to the shared slot. But, the beam steering behavior is stable across the bandwidth and good results were obtained.

The radiation patterns for each individual port were measured for the co-pol and cross-pol configurations, and then the patterns were combined using MATLAB due to the lack of an available beamformer. Fig. 11 shows the radiation pattern measurement setups for the two bands of operation. The lower band (sub-6GHz) was measured in a near-field setup (a Satimo Star-Lab) as shown in Fig. 11(a), while the mm-wave patterns were measured in a quasi-far field compact range as shown in Fig. 11(b). The pattern combining process took care of the phase differences between various feeding paths to make sure proper phases are provided to steer the beam in the proper direction. The patterns were measured at 27, 28, 29 30 and 31 GHz for each port. Figures 12 and 13 show the element normalized patterns for the 4 ports at 27 and 31 GHz, respectively. Good agreement is observed in general with a little bit a ripple in the measured results in the main lobe direction that is due to the measurement setup used (the phase-locked loop filter did not have good performance in the chamber used). Also, sometimes the main beam is wider with higher levels in the measurements, and that might be attributed to the presence of cables, the complete metal frame and feeding mast that do not exist in the simulation model. Such effects will have less impact when the beams are combined which is the case for all mm-wave arrays as will be seen in the combined patterns in the figures to come. The efficiency of the SB-CAA antenna was better than 85%.

To examine the beam steering capability of this mm-wave array, the beams were combined to steer the beam

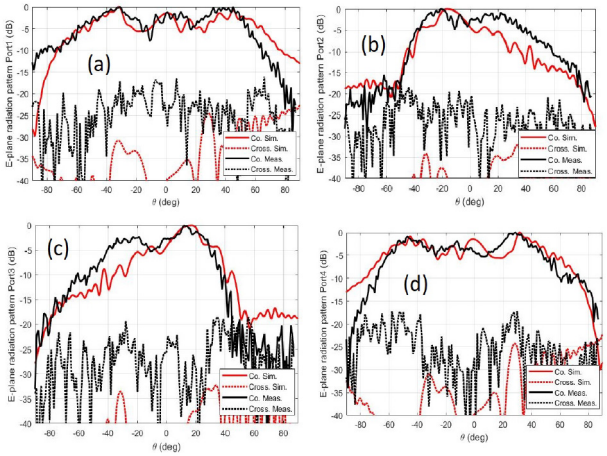

FIGURE 12. Normalized radiation patterns (co-pol and cross-pol) for the single SB-CAA at 27 GHz (a) port 1, (b) port 2, (c) port 2 and (d) port 4.

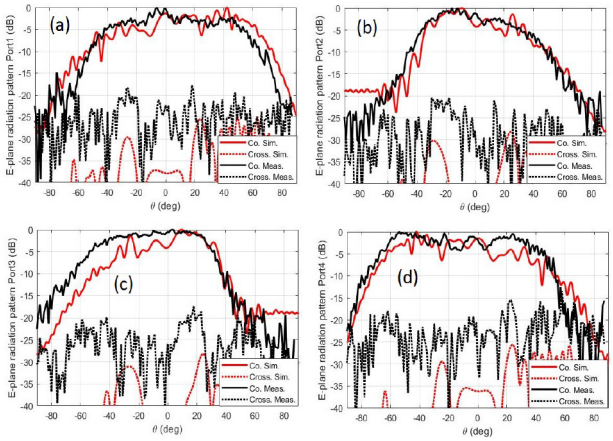

FIGURE 13. Normalized radiation patterns (co-pol and cross-pol) for the single SB-CAA at 31 GHz (a) port 1, (b) port 2, (c) port 2 and (d) port 4.

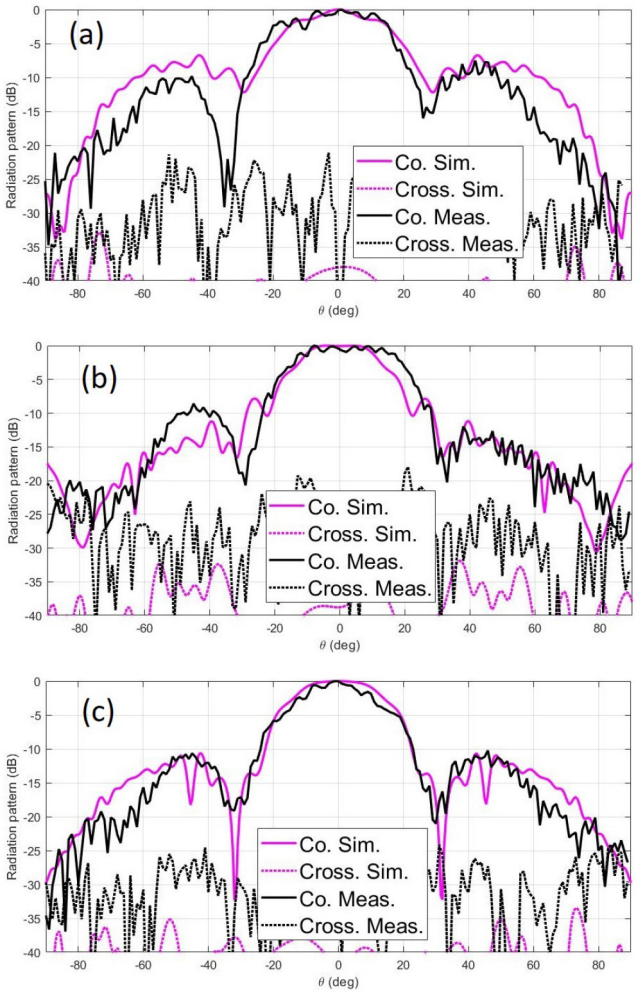

FIGURE 14. Normalized radiation patterns (co-pol and cross-pol) simulated and measured for the single SB-CAA at Boresight (all ports combined), (a) at 27 GHz, (b) 29 GHz and (c) at 31 GHz radiation patterns (co-pol and cross-pol) for the single SB-CAA at 27 GHz (a) port 1, (b) port 2, (c) port 2 and (d) port 4.

towards +/- 30 degrees. The comparison between the simulated and measured combined patterns at boresight are shown in Fig. 14 for the frequencies of 27, 29 and 31 GHz. The measured patterns show side lobe levels lower than 8-9 dB for all cases. The maximum gain at boresight as a function of frequency is shown in Fig. 15. As can be seen, the simulated and measured gains are in good agreement over the wide-band of operation (26 – 30 GHz). It should be noted that gain values beyond 30 GHz in simulations are not accurate due to the poor matching that occurs at ports 1 and 4.

The results of this beam steering are shown in Fig. 16 showing the beam steering at the two frequencies of 27 and 31 GHz. The beam was steered between 0 to -30 degrees (similar results are seen between 0 and 30 degrees due to the symmetry in the structure) with good SLL and gain. The gain degradation at -30 degrees was 1 dBi and 2.5 dBi at the 27 GHz and 31 GHz bands, respectively, showing good beam steering performance from a 4-element linear array.

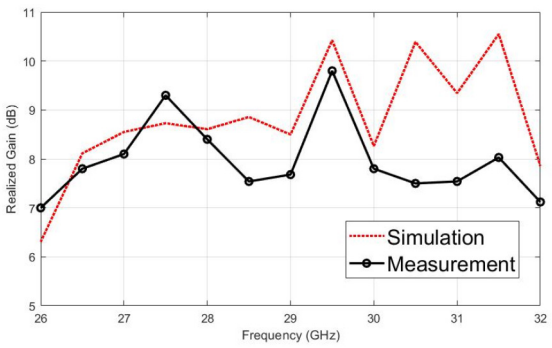

FIGURE 15. Realized gain of the single SB-CAA at Boresight as a function of frequency.

C. RESULTS FOR THE SA CACTUS-BASED ANTENNA

The measured and simulated S-parameters for the SA cactus shaped antenna for the sub-6 GHz and mm-wave bands are shown in Fig. 17. The performance of the sub-6 GHz portion is shown in Fig. 17 (a), where it covered the bands

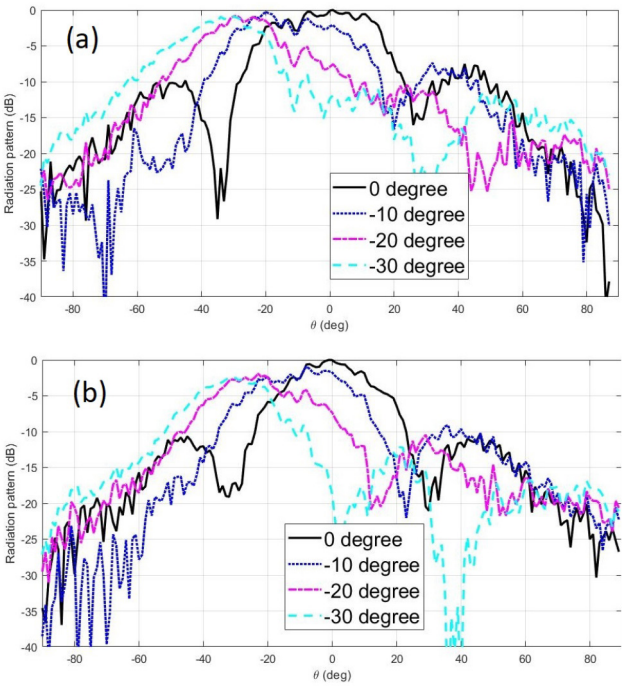

FIGURE 16. Measured normalized beam steering performance of the single SB-CAA, (a) at 27 GHz, (b) at 31 GHz.

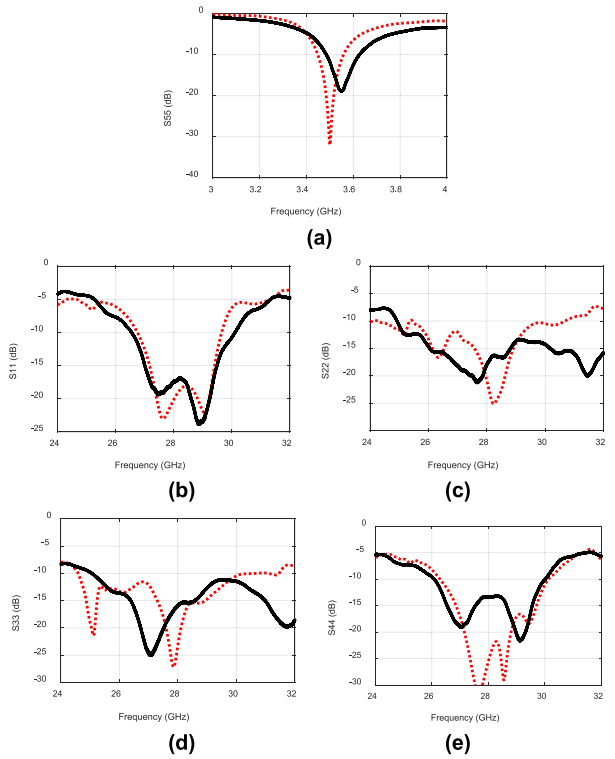

FIGURE 17. Simulated (dashed line) and Measured (solid line) S-parameters for the SA-Cactus shaped antenna, (a) microwave band (port 5), (b) port 1, (c) port 2, (d) port 3 and (e) port 4.

between 3.48-3.62 GHz in measurements as compared to 3.45 – 3.56 GHz in simulations. For the mm-wave array (Figs. 17 (b)-(e)), the minimum measured frequency range

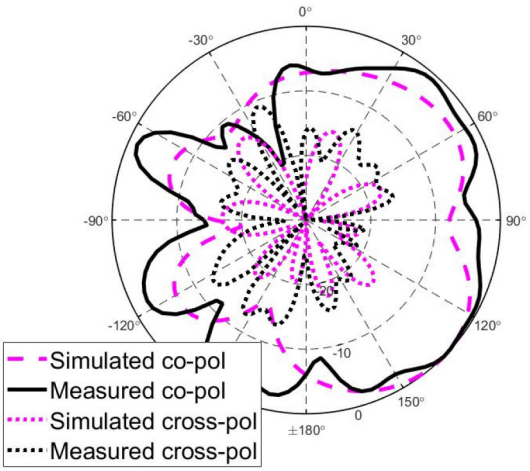

FIGURE 18. Simulated (magenta dashed line) and Measured (black solid line) co-pol (E-plane) gain pattern for the SA-Cactus shaped antenna at 3.55 GHz (P5 for microwave band).

(was for P1) was 26.52 – 30.14 GHz as compared to its simulation counterpart of 26.7 – 29.7 GHz. Very good agreement and wide bandwidth was obtained from this small size SA antenna structure.

The measured co-pol and cross-pol normalized gain patterns for E-plane (see Fig. 5) of the microwave band of the SA cactus shaped antenna are shown in Fig. 18 at the center frequency of 3.55 GHz. The maximum gain was around 2.5 dBi. The total efficiency was better than 90%.

For the mm-wave CAA of the SA cactus antenna, the individual patterns were measured and then post processed for beamforming capability. The measured and simulated array patterns at Boresight are shown in Fig. 19 for the two frequencies of 27.5, 28.5 and 29.5 GHz. Very good agreement is observed. The beamforming capability of the CAA within the SA cactus antenna was investigated and good performance between +/- 30 degrees in terms of gain and SLL was observed. The tilted measured beams are shown in Fig. 20 for the two frequencies of 27.5 and 29.5 GHz. At higher frequencies, the main beam suffers a little bit from a dip that originates from the two middle elements (P2 and P3) because of the connection with the upper slot. The maximum realized gain values from measurements and simulations are presented in Fig. 21. Good agreement is observed over a wideband. The average gain is approximately 8 dBi for this 4-element CAA array. The efficiency of the mm-wave CAA array within the SA cactus shaped antenna was higher 75% over the entire band of operation.

A table of comparison with most recent dual band antenna systems covering the sub-6 GHz and mm-wave bands of the 5G standard is presented in Table 3. It is clear that the proposed designs; the single SB-CAA and the SA cactus shaped, has the unique features of extremely small aperture area sizes, good steering angle capabilities, and excellent bandwidth performance with the fact

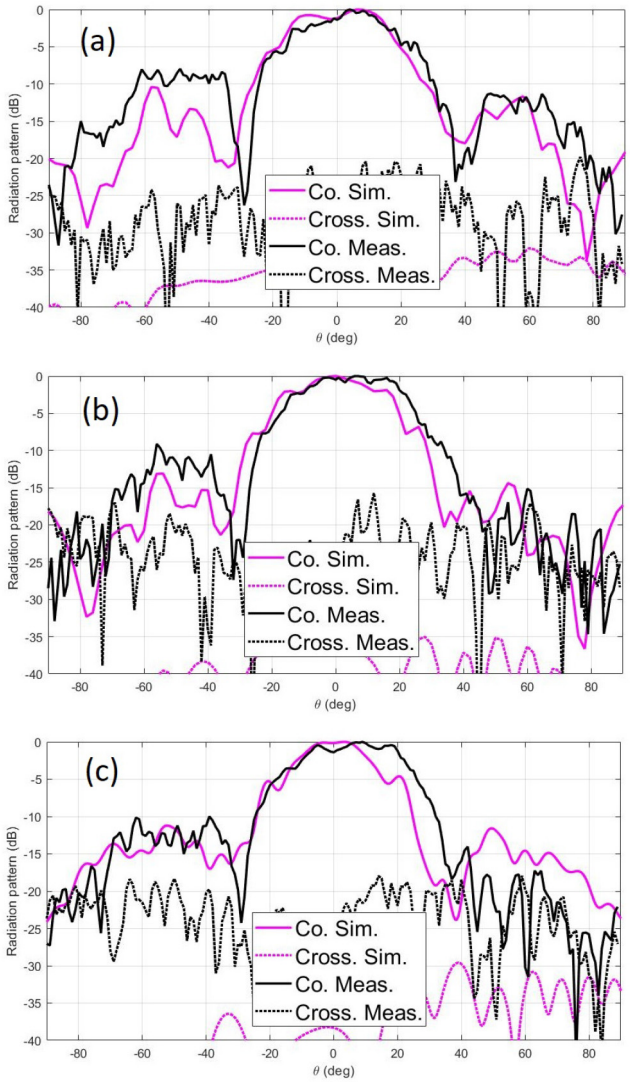

FIGURE 19. Normalized radiation patterns (co-pol and cross-pol) simulated and measured for the 4-element CAA within the SA cactus shaped antenna at Boresight (all ports combined), (a) at 27.5 GHz, (b) at 28.5 GHz and (c) 29.5 GHz.

that it will be part of the metal rim thus providing high integration advantage as compared to PCB based ones listed.

The fact that the proposed antennas (SB-CAA or the SA cactus shaped) are small is size (and area), multiple slots within the rim on its various sides can easily provide a mm-wave multiple-input-multiple-output (MIMO) antenna configurations that is essential and is required at mm-wave bands. This can also reduce the performance degradation suffered when an antenna is blocked by the user hand. Several previous proposed designs do not have this capability as they are based on large size PCB based designs that might require large openings within the metal frame to allow for proper radiation and beam steering, or they are already occupying large areas on phone edges as shown in [20]. Thus, another evident advantage of the proposed structure.

TABLE 3. A comparison summary between previous works that consider sub-6GHz and mm-wave design.

Ref.	Frequency bands (GHz)	BW (GHz)	Peak Realized Gain (dBi)	Radiator Size / slot opening (mm^2)	Antenna Type / Number of elements	Beam steering Capability (measured)
[8]	2 / 24 / 28	~ 0.06 / 1.5 / 2.6	4.5 / 12.2 / 12.1	35×2.5 (87.5)	Single slot / 8-element CAA	No
[11]	0.8 / 2.2 / 27.5	0.26 / 1 / 5	- / - / 7	91 x 7 (637) (sub-6) / 4 x 23 (92) (mm-wave)	Multi-fed metal edge / 4-element vivaldi	No
[14]	3.5 / 28	0.51 / 5.44	7.1 / 11.3	33.9 × 43 (1457.7)	Dipole / 4-element Yagi	±25°
[15]	3.5 / 26	0.43 / 3.4	5.3 / 13.9	35 × 25 × 2.74 (875) (3D structure)	Patch / 8-element SIDRA	±25°
[19]	0.85 / 1.95 / 26.5	0.22 / 0.5 / 9	0.3 / 3.6 / 9.5	70 x 9 (630)	PIFA / 4-element Folded Dipoles	±50°
[20]	0.875 \ 3.35 \ 27.9	0.17 \ 3.3 \ 0.85	2.5 \ 5.5 \ 7.5	34 x 8 (272)	CCE / Parasitic reconfigurable patches	±45° (each corner, totaling to 90°)
This work	**(a) Single SB-CAA (28)** **(b) SA Cactus (3.5 / 28)**	**(a) 6** **(b) 0.14 / 3.5**	**(a) 10.2** **(b) 2.5 @ 3.5 / 9.8 @ 28**	**(a) 17.8 x 2 (35.6)** **(b) 26.8 x 3.8* (slot area is 33.12)**	**(a) SB-CAA 4-elements** **(b) SA cactus slot (microwave and mm-wave)**	**±30°**

*Note that this is not the rim clearance or total area of the aperture, but rather the outer area of the structure. The actual slot area (aperture area) needed by the proposed antenna is much less which is only 33.12 mm2. Please see Fig. 4.

IV. CONCLUSION

This work presents for the first time a slot based shared aperture antenna system covering the 3.5 GHz and 28GHz bands of the 5G wireless standard. The proposed antenna is

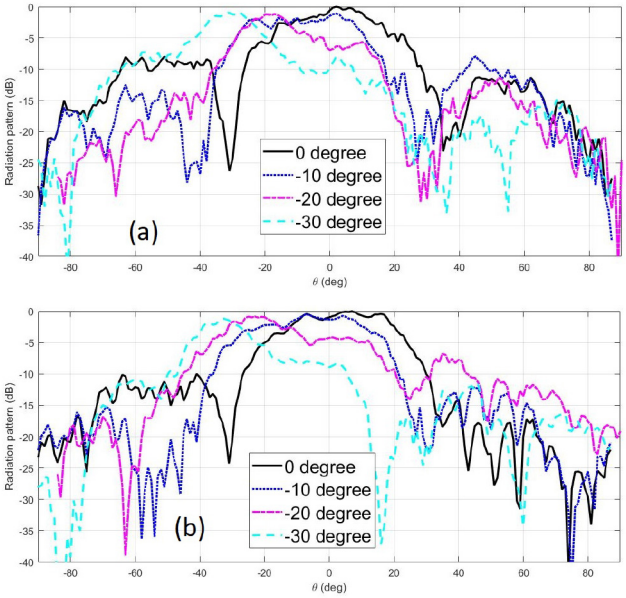

FIGURE 20. Normalized measured radiation patterns for the 4-element CAA within the SA cactus shaped antenna with beam steering (all ports combined), (a) at 27.5 GHz, (b) at 29.5 GHz.

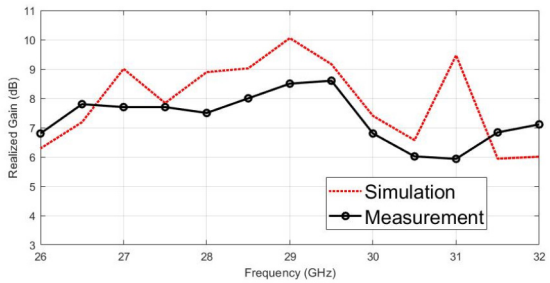

FIGURE 21. Measured and simulated realized gain (dBi) values at Boresight as a function of frequency for the SA cactus shaped antenna for the 4-element CAA at mm-wave bands.

a SA cactus shaped slot based antenna that is directly etched out from the metal rim (metal frame) of a mobile terminal. The proposed design provides more than 140 MHz of frequency bandwidth in the sub-6 GHz band, and more than 3.5 GHz of bandwidth in the 28 GHz band. The mm-wave portion of the antenna is based on a CAA with beam steering capability. The beam can be steered between +/− 30 degrees. The area of the SA cactus slot based antenna is only 33.12 mm2, which is way much smaller than any other present solution. A mm-wave only SB-CAA with beam steering capability is also proposed that operated also at 28 GHz and provided more than 6 GHz of frequency bandwidth. Both antenna systems were placed on a mobile phone metal rim. The peak measured gains for the sub-6GHz and 28 GHz bands for the SA cactus antennas were 2.5 and 9.8 dBi, respectively. Excellent efficiency for all antennas within all bands was achieved which exceeded 75%.

REFERENCES

[1] E. G. Larsson and L. Van der Perre, "Massive MIMO for 5G," *IEEE 5G Tech Focus*, vol. 1, no. 1, pp. 1–4, Mar. 2017.

[2] D. Cavallo, A. Neto, G. Gerini, A. Micco, and V. Galdi, "A 3-to 5-GHz wideband array of connected dipoles with low cross polarization and wide-scan capability," *IEEE Trans. Antennas Propag.*, vol. 61, no. 3, pp. 1148–1154, Mar. 2013.

[3] Q. Chen, H. Lin, J. Wang, L. Ge, Y. Li, and T. Pei, "Single ring slot-based antennas for metal-rimmed 4G/5G smartphones," *IEEE Trans. Antennas Propag.*, vol. 67, no. 3, pp. 1476–1487, Mar. 2019.

[4] R. M. Moreno *et al.*, "Dual-polarized mm-Wave endfire chain-slot antenna for mobile devices," *IEEE Trans. Antennas Propag.*, vol. 69, no. 1, pp. 25–34, Jan. 2021.

[5] R. M. Moreno, J. Ala-Laurinaho, A. Khripkov, J. Ilvonen, and V. Viikari, "Dual-polarized mm-wave endfire antenna for mobile devices," *IEEE Trans. Antennas Propag.*, vol. 68, no. 8, pp. 5924–5934, Aug. 2020.

[6] J. Choi *et al.*, "Frequency-adjustable planar folded slot antenna using fully integrated multithrow function for 5G mobile devices at millimeter-wave spectrum," *IEEE Trans. Microw. Theory Techn.*, vol. 68, no. 5, pp. 1872–1881, May 2020.

[7] R. M. Moreno, J. Ala-Laurinaho, and V. Viikari, "Dual-polarized mm-Wave antenna solution for mobile phone," in *Proc. 14th Eur. Conf. Antennas Propag. (EuCAP)*, 2020, pp. 1–5.

[8] M. Ikram, E. Al Abbas, N. Nguyen-Trong, K. H. Sayidmarie, and A. Abbosh, "Integrated frequency-reconfigurable slot antenna and connected slot antenna array for 4G and 5G mobile handsets," *IEEE Trans. Antennas Propag.*, vol. 67, no. 12, pp. 7225–7233, Dec. 2019.

[9] M. S. Sharawi, M. Ikram, and A. Shamim, "A two concentric slot loop based connected array MIMO antenna system for 4G/5G terminals," *IEEE Trans. Antennas Propag.*, vol. 65, no. 12, pp. 6679–6686, Dec. 2017.

[10] M. Ikram, R. Hussain, and M. S. Sharawi, "4G/5G antenna system with dual function planar connected array," *IET Microw. Antennas Propag.*, vol. 11, no. 12, pp. 1760–1764, 2017.

[11] J. Kurvinen, H. Kähkönen, A. Lehtovuori, J. Ala-Laurinaho, and V. Viikari, "Co-designed mm-Wave and LTE handset antennas," *IEEE Trans. Antennas Propag.*, vol. 67, no. 3, pp. 1545–1553, Mar. 2019.

[12] M. Ikram, M. Sharawi, A. Shamim, and A. Sebak, "A multiband dual-standard MIMO antenna system based on monopoles (4G) and connected slots (5G) for future smart phones," *Microw. Opt. Technol. Lett.*, vol. 60, no. 6, pp. 1468–1476, 2018.

[13] R. Hussain, A. T. Alreshaid, S. K. Podilchak, and M. S. Sharawi, "Compact 4G MIMO antenna integrated with a 5G array for current and future mobile handsets," *IET Microw. Antennas Propag.*, vol. 11, no. 2, pp. 271–279, 2017.

[14] J. Lan, Z. Yu, J. Zhou, and W. Hong, "An aperture-sharing array for (3.5, 28) GHz terminals with steerable beam in millimeter-wave band," *IEEE Trans. Antennas Propag.*, vol. 68, no. 5, pp. 4114–4119, May 2020.

[15] X.-H. Ding, W.-W. Yang, W. Qin, and J.-X. Chen, "A broadside shared aperture antenna for (3.5, 26) GHz mobile terminals with steerable beam in millimeter-waveband," *IEEE Trans. Antennas Propag.*, vol. 70, no. 3, pp. 1806–1815, Mar. 2022.

[16] Y. Wang, H.-C. Huang, and X. Jian, "Novel design of a dual-band 5G mm-Wave antenna array integrated with a metal frame of a cellular phone," in *Proc. Asia-Pacific Microw. Conf. (APMC)*, 2018, pp. 1582–1584.

[17] H.-C. Huang, Y. Wang, and X. Jian, "Novel integrated design of dual-band dual-polarization mm-Wave antennas in non-mm-Wave antennas (AiA) for a 5G phone with a metal frame," in *Proc. Int. Workshop Antenna Technol. (iWAT)*, 2019, pp. 125–128.

[18] A. Neto and J. Lee, "Ultrawide-band properties of long slot arrays," *IEEE Trans. Antennas Propag.*, vol. 54, no. 2, pp. 534–543, Feb. 2006.

[19] M. M. S. Taheri, A. Abdipour, S. Zhang, and G. F. Pedersen, "Integrated millimeter-wave wideband end-fire 5G beam steerable array and low-frequency 4G LTE antenna in mobile terminals," *IEEE Trans. Veh. Technol.*, vol. 68, no. 4, pp. 4042–4046, Apr. 2019.

[20] Q. Liang and B. K. Lau, "Co-designed millimeter-wave and sub-6GHz antenna for 5G smartphones," *IEEE Antennas Wireless Propag. Lett.*, early access, Jul. 1, 2022, doi: 10.1109/LAWP.2022.3187782.

REZA SHAMSAEE MALFAJANI (Graduate Student Member, IEEE) received the B.S. degree in electrical engineering from the University of Tehran, Tehran, Iran, in 2009, and the M.S. degree in electrical engineering from Tarbiat Modares University, Tehran, in 2012. He is currently pursuing the Ph.D. degree with Polytechnique Montréal, Montreal, QC, Canada, where he is also a member of the Poly-Grames Research Center. His research focuses on the periodic structures, antennas and RF, mm-wave, and Terahertz designs.

FARHAD BIN ASHRAF was born in Chittagong, Bangladesh, in 1991. He received the B.Sc. degree in electrical and electronic engineering from International Islamic University Chittagong in 2015, the Master of Science degree in electrical, electronic and systems engineering from Universiti Kebangsaan Malaysia in 2019, and the Master of Applied Science degree in electrical engineering from Polytechnique Montréal in 2022. His publication includes 8 research journal papers, nearly 10 conference papers, and two book chapters on various topics related to antennas, metamaterials, sensors, microwaves, and electromagnetic radiation analysis. His research interests include the 5G antenna, mmWave, metamaterial applications, electromagnetic radiation, and electromagnetic compatibility.

MOHAMMAD S. SHARAWI (Senior Member, IEEE) is a Full Professor with the Electrical Engineering Department, University of Montréal (Polytechnique Montréal), Montreal, QC, Canada, where he is also a member of the Poly-Grames Research Center. He was with the King Fahd University of Petroleum and Minerals (KFUPM), Dhahran, Saudi Arabia, from 2009 to 2018. He founded and directed the Antennas and Microwave Structure Design Laboratory, KFUPM. He was a Visiting Professor with the Intelligent Radio Laboratory, Department of Electrical Engineering, University of Calgary, Calgary, AB, Canada, in the Summer-Fall of 2014. He was a Visiting Research Professor with Oakland University, Rochester, MI, USA, in the Summer of 2013. He has more than 350 papers published in refereed journals and international conferences, 11 book chapters (two of which in the Antenna Handbook, 5th edition, McGraw Hill, 2018), one single authored book entitled *Printed MIMO Antenna Engineering*, Artech House, 2014, and the Lead Author of the recent book *Design and Applications of Active Integrated Antennas*, Artech House, 2018. He has 25 issued/granted and 12 pending patents in the U.S. Patent Office. His research interests include multiband printed multiple-input-multiple-output (MIMO) antenna systems, reconfigurable and active integrated antennas, millimeter-wave MIMO antennas and integrated 4G/5G antennas, microwave sensors, applied electromagnetics, and computational methods. He was a recipient of the Abdul Hameed Shoman Foundation Award (AHSF) for Arab researchers for the category of wireless systems in 2020 in addition to various best IEEE conference paper awards. He is also serving as the Associate Editor for the IEEE ANTENNAS AND WIRELESS PROPAGATION LETTERS, IET MICROWAVES, ANTENNAS AND PROPAGATION, and IEEE OPEN JOURNAL ON ANTENNAS AND PROPAGATION; and an Area Editor (Antennas and Microwave Devices and Systems) for *Microwave and Optical Technology Letters*. He is also the Specialty Chief Editor for the newly launched Frontiers in *Communications and Networks* journal for the System and Test-Bed Design Section. He has served on the Technical and organizational program committees and organized several special sessions on MIMO antenna systems and architectures in several international conferences, such as EuCAP, APS, IMWS-5G, APCAP, and iWAT among many others for many years. He is also the IEEE Antennas and Propagation Society (APS) Chair of the Montreal section and an active member of the IEEE Member benefits committee leading the initiative of the APS Student Travel Grant. He is also the regional delegate of the EuRAAP in North America.